

SUPPORTING INFORMATION

Does it mix? Insights and attempts to predict the formability of single phase mixed A-cation lead iodide perovskites

F. B. Minussi^{1*}, R. M. Silva Jr.², E. B. Araújo¹

¹ Department of Physics and Chemistry, São Paulo State University, 15385-000, Ilha Solteira, SP, Brazil

² Department of Electrical Engineering, São Paulo State University, 15385-000, Ilha Solteira, SP, Brazil

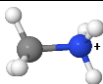
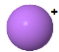
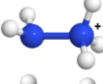
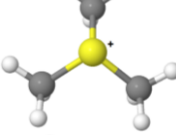
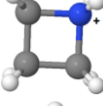
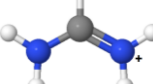
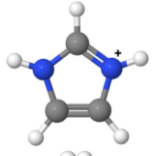
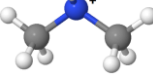
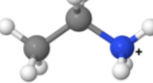


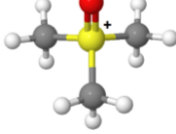
CONTENTS

Supplementary Note 1: Typical A-site cations used in halide perovskites	S1
Supplementary Note 2: Data used to construct tolerance factor plots	S2
Supplementary Note 3: Graphical visualization of descriptors	S5
Supplementary Note 4: Confidence ellipses	S6
Supplementary Note 5: Additional X-ray diffraction data	S7
Supplementary Note 6: Entropy of mixing	S8
References	S9

* corresponding author: f.minussi@unesp.br

Supplementary Note 1: Typical A-site cations used in halide perovskites

Table S1 - Ionic radius (r_A), dipole moment (μ_A) and the number of N-H bonds (n_{NH}) of some A-site cations used in halide perovskites. Dipole moment values were calculated using MolCalc [1].

Cation	Structure	Symbol	r_A (pm)	μ_A (D)	n_{NH}
methylammonium		MA ⁺	217 ^[2]	2.69	3
cesium		Cs ⁺	188 ^[3]	0	0
hydrazinium		HY ⁺	217 ^[2]	3.50	5
trimethylsulfonium		TMS ⁺	244 ^[4]	1.08	0
azetidinium		AZ ⁺	250 ^[2]	3.83	2
formamidinium		FA ⁺	253 ^[2]	0.22	4
imidazolium		IM ⁺	258 ^[2]	1.99	2
dimethylammonium		DMA ⁺	272 ^[2]	1.93	2
ethylammonium		EA ⁺	274 ^[2]	4.97	3
acetamidinium		AC ⁺	277 ^[5]	2.01	4
guanidinium		GA ⁺	278 ^[2]	0	6
trimethylsulfoxonium		TMSO ⁺	289 ^[6]	5.80	0

Supplementary Note 2: Data used to construct tolerance factor plots

To calculate the Goldschmidt (t) and Bartel (τ) tolerance factors of $A_xMA_{1-x}PbI_3$ compounds, we used the relations respectively given by

$$t = \frac{(r_{eff} + r_X)}{\sqrt{2}(r_B + r_X)}$$

$$\tau = \frac{r_X}{r_B} - n_A \left[n_A - \frac{(r_{eff}/r_B)}{\ln(r_A/r_B)} \right]$$

where r_{eff} , r_B and r_X are the ionic radii of the cations at the A, B, and X sites and n_A is the oxidation number of the A-site cation. For solid solutions, effective ionic radii at the A-site were calculated using the relation $r_{eff} = xr_A + (1 - x)r_{MA}$, where r_A and r_{MA} are the ionic radius of substituent cation A^+ and of MA^+ , respectively, and x is the molar fraction of substitution. Ionic radii of A-site cations are given in Table S1. The radii used for $B = Pb^{2+}$ and $X = I^-$ were 119 and 220 pm [3], respectively. Calculated t and τ values for compositions with experimental phase purity data are given in Table S2.

Table S2 - Calculated and experimental information on $A_xMA_{1-x}PbI_3$ solid solutions. Methods are XRD: X-ray diffraction, UVS: UV-Vis spectroscopy and NMR: nuclear magnetic resonance.

A^+	x	t	τ	A-site segregate?	Method	Reference
-	0	0.912	3.884	-	-	-
Cs^+	0.05	0.908	3.898	Yes ($CsPbI_3$)	XRD	[7]
	0.1	0.905	3.912	Yes ($CsPbI_3$)	XRD	[7]
	0.2	0.899	3.942	Yes ($CsPbI_3$)	XRD	[7]
	0.3	0.893	3.975	Yes ($CsPbI_3$)	XRD	[7]
	0.4	0.887	4.011	Yes ($CsPbI_3$)	XRD	[7]
HY^+	0.1	0.912	3.884	No	UVS	[8]
	0.2	0.912	3.884	No	UVS	[8]
	0.3	0.912	3.884	No	UVS	[8]
	0.4	0.912	3.884	Yes ($HYPbI_3$)	UVS	[8]
	0.5	0.912	3.884	Yes ($HYPbI_3$)	UVS	[8]
TMS^+	0.025	0.913	3.878	Yes ($TMSPbI_3$)	XRD	[6]
	0.033	0.913	3.876	Yes ($TMSPbI_3$)	XRD	[6]
	0.046	0.914	3.873	Yes ($TMSPbI_3$)	XRD	[6]
AZE^+	0.01	0.912	3.881	No	UVS/XRD	[9]
	0.02	0.913	3.878	No	UVS/XRD	[9]
	0.05	0.915	3.869	Yes ($AZEPbI_3$)	UVS/XRD	[9]
	0.10	0.918	3.855	Yes ($AZEPbI_3$)	UVS/XRD	[9]

Table S2 - Continued.

AZE ⁺	0.25	0.929	3.815	Yes (AZEPbI ₃)	UVS/XRD	[9]
FA ⁺	0.050	0.915	3.868	No	XRD	[10]
	0.075	0.917	3.860	No	XRD	[10]
	0.10	0.919	3.852	No	XRD	[11]
	0.125	0.921	3.845	No	XRD	[10]
	0.15	0.923	3.837	No	XRD	[10]
	0.175	0.925	3.830	No	XRD	[10]
	0.20	0.927	3.823	No	XRD	[11]
	0.30	0.934	3.797	No	XRD	[11]
	0.40	0.942	3.773	No	XRD	[11]
	0.50	0.949	3.751	No	XRD	[11]
IM ⁺	0.10	0.920	3.848	No	XRD	[12]
	0.20	0.929	3.816	Yes (IMPbI ₃)	XRD	[12]
	0.30	0.937	3.786	Yes (IMPbI ₃)	XRD	[12]
DMA ⁺	0.05	0.917	3.859	No	NMR	[13]
	0.10	0.923	3.836	No	NMR	[13]
	0.15	0.929	3.815	No	NMR	[13]
	0.20	0.934	3.795	No	NMR	[13]
	0.25	0.940	3.777	Yes (DMAPbI ₃)	NMR	[13]
EA ⁺	0.09	0.922	3.839	No	NMR/XRD	[14]
	0.10	0.923	3.835	No	UVS/XRD	[15]
	0.16	0.931	3.809	No	NMR/XRD	[14]
	0.20	0.935	3.793	No	UVS/XRD	[15]
	0.21	0.936	3.789	No	NMR/XRD	[14]
	0.30	0.947	3.756	No	UVS/XRD	[15]
	0.31	0.948	3.753	No	NMR/XRD	[14]
	0.38	0.957	3.731	No	NMR/XRD	[14]
	0.40	0.959	3.725	Yes (EAPbI ₃)	UVS/XRD	[15]
	0.50	0.971	3.698	Yes (EAPbI ₃)	UVS/XRD	[15]
AC ⁺	0.10	0.924	3.833	No	XRD	[16]
	0.20	0.937	3.789	Yes (ACPbI ₃)	XRD	[16]
	0.30	0.949	3.751	Yes (ACPbI ₃)	XRD	[16]
GA ⁺	0.025	0.915	3.870	No	XRD	[17]
	0.05	0.918	3.857	No	XRD	[17]
	0.075	0.921	3.844	No	XRD	[17]
	0.10	0.924	3.832	No	XRD	[17]

Table S2 - Continued.

	0.125	0.927	3.820	No	XRD	[17]
	0.15	0.931	3.809	No	XRD	[17]
	0.175	0.934	3.798	No	XRD	[17]
GA ⁺	0.20	0.937	3.787	No	XRD	[18]
	0.25	0.943	3.767	No	XRD	[17]
	0.30	0.950	3.749	Yes (GAPbI ₃)	XRD	[18]
	0.40	0.962	3.717	Yes (GAPbI ₃)	XRD	[18]
	0.50	0.975	3.689	Yes (GAPbI ₃)	XRD	[17]
	0.025	0.915	3.868	No	XRD	[6]
TMSO ⁺	0.033	0.916	3.863	Yes (TMSOPbI ₃)	XRD	[6]
	0.046	0.918	3.855	Yes (TMSOPbI ₃)	XRD	[6]

Supplementary Note 3: Graphical visualization of descriptors

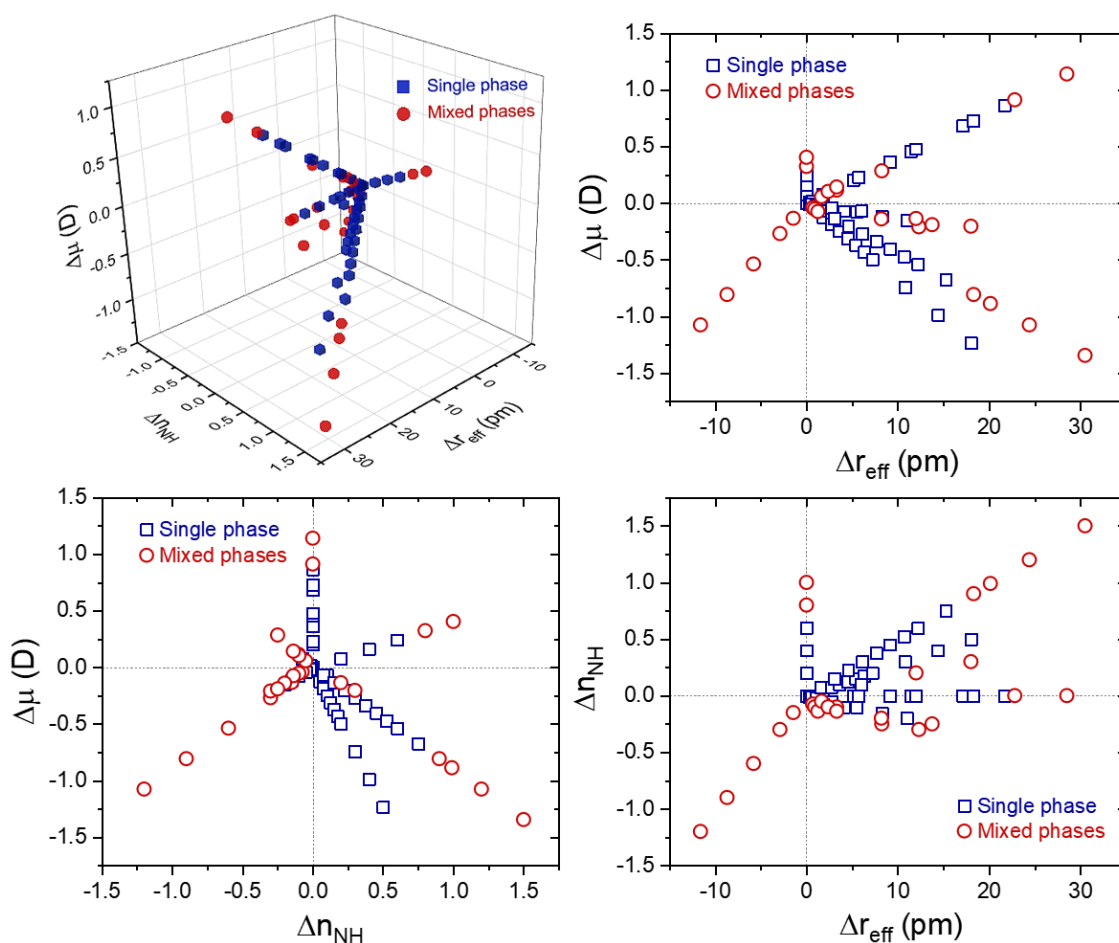


Figure S1 - 3D and 2D plots of physical descriptors proposed in this work. Note that the dipole moment descriptor ($\Delta\mu$) doesn't provide any benefit for separating single phase from mixed phases data; data for both cases are encountered regardless if $\Delta\mu$ is close or not to the origin or if it is positive or negative.

Supplementary Note 4: Confidence ellipses

Statistically calculated confidence ellipses for Δn_{NH} versus Δr_{eff} data are shown in Figure S2. In summary, these ellipses are ineffective in separating single and mixed-phase data because they are calculated to maximize the inclusion of a desired data set inside the region delimited by the ellipse under a given confidence level. By doing so, undesired data is included inside the ellipse (higher confidence levels) or desired data is not inside the ellipse (lower confidence levels). On the other hand, even if an optimal confidence level could be found, calculated ellipses are always rotated, which is unsuitable since we were aiming for the simplest equation possible. Clustering methods don't seem adequate as well because the data of mixed phases are too dispersed.

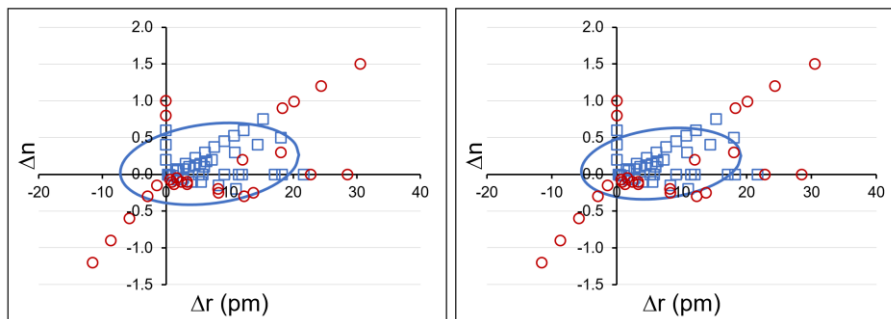


Figure S2 - Confidence ellipses of 95% (left) and 90% (right) levels. Blue and red dots are of single and mixed phases data, respectively.

Supplementary Note 5: Additional X-ray diffraction data

To complement the solubility diagram, we synthesized twelve $\text{GA}_x\text{FA}_y\text{MA}_{1-x-y}\text{PbI}_3$ compositions. Amounts of the precursors lead iodide (PbI_2 , Sigma-Aldrich, 99%), methylammonium iodide ($\text{CH}_3\text{NH}_3\text{I}$ or MAI, Sigma-Aldrich, 98%), formamidinium iodide ($\text{CH}(\text{NH}_2)_2\text{I}$ or FAI, Sigma-Aldrich, 99%), and guanidinium iodide ($\text{C}(\text{NH}_2)_3\text{I}$ or GAI, Sigma-Aldrich, 99%) were weighted in desired proportions. The precursors were manually mixed and ground to react in a natural agate mortar for about one hour under ambient conditions. The resulting black powders of perovskites were sieved in a 250 μm aperture sieve, dried, and annealed for 6 h at 333 K in a laboratory oven with periodic (once an hour) stirring. Pelletized powders were produced with approximately 180 mg of the as-synthesized powders uniformly spread into a 10 mm diameter circular cavity of a metallic mold and compacted with a pressure of about 250 MPa. X-ray diffraction measurements (XRD) were performed in these pellets using a Rigaku Ultima IV diffractometer with $\text{CuK}\alpha$ radiation ($\lambda = 1.5406 \text{ \AA}$), under 40 kV and 20 mA, with a continuous scan (2° min^{-1}), in the range of 2θ from 10 to 16° under controlled conditions (dark, at $\sim 300 \text{ K}$ and relative humidity below 30%). Results are shown in Figure S3.

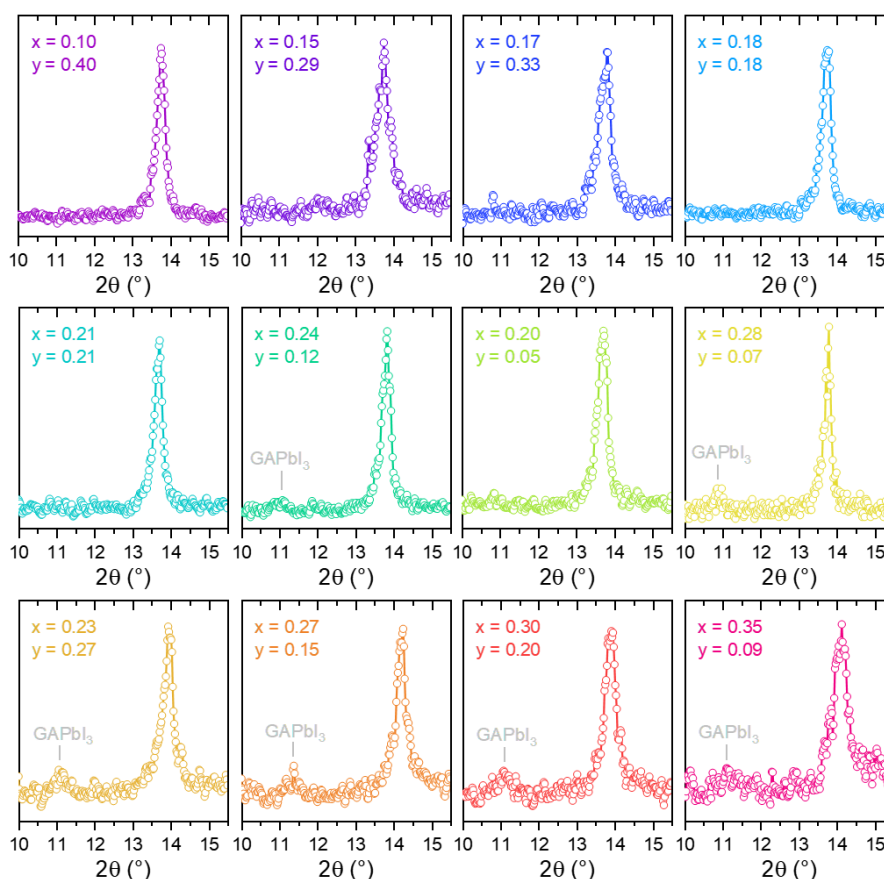


Figure S3 - XRD data of the synthesized $\text{GA}_x\text{FA}_y\text{MA}_{1-x-y}\text{PbI}_3$ compositions.

Supplementary Note 6: Entropy of mixing

To picture the changes in the entropy of mixing in $\text{GA}_x\text{FA}_y\text{MA}_{1-x-y}\text{PbI}_3$ compositions, we used the classical approach of considering an entirely random of solutes under constant temperature, volume and pressure. The entropy of mixing in this ideal case can be given by

$$\Delta S_{mix} = -R[x \ln x + y \ln y + z \ln z]$$

where R is the universal gas constant and x , y and $z = 1 - x - y$ are the mole fractions of GA^+ , FA^+ and MA^+ . The ternary diagram of ΔS_{mix} is given in Figure S4.

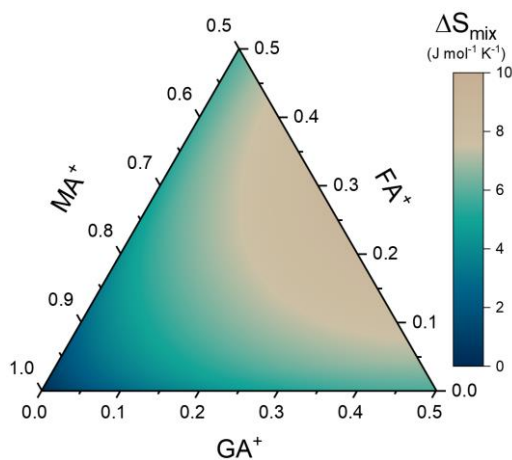


Figure S4 - Composition-dependent entropy of mixing in an ideal ternary $\text{GA}_x\text{FA}_y\text{MA}_{1-x-y}\text{PbI}_3$ system.

References

- [1] J. H. Jensen and J. C. Kromann, *J. Chem. Educ.*, 2013, 90, 1093.
- [2] G. Kieslich, S. Sun, and Anthony K. Cheetham, *Chem. Sci.*, 2015, 6, 3430.
- [3] R. D. Shannon, *Acta Crystallogr., Sect. A: Found. Adv.*, 1976, 32, 751.
- [4] A. Kaltzoglou et al., *Inorg. Chem.*, 2017, 56, 6302–6309.
- [5] P. Singh et al., *ACS Appl. Mater. Interfaces*, 2020, 12, 13982.
- [6] M. Parashar et al., *ACS Appl. Energy Mater.*, 2021, 4, 2751.
- [7] H. Choi et al., *Nano Energy*, 2014, 7, 80.
- [8] A. F. Akbulatov et al., *J. Mater. Chem. A*, 2016, 4, 18378.
- [9] S. R. Pering et al., *J. Mater. Chem. A*, 2017, 5, 20658.
- [10] A. Mohanty et al., *ACS Energy Lett.*, 2019, 4, 2045.
- [11] O. J. Weber, B. Charles, and M. T. Weller, *J. Mater. Chem. A*, 2016, 4, 15375.
- [12] Yi Zhang et al., *Nano Energy*, 2019, 58, 105.
- [13] W. M. J. Franssen et al., *Inorg. Chem.*, 2020, 59, 3730.
- [14] Mantas Šimėnas et al., *Chem. Mater.*, 2022, 34, 10104.
- [15] Yong Wang et al., *J. Energy Chem.*, 2018, 27, 215.
- [16] Pallavi Singh et al., *ACS Appl. Mater. Interfaces*, 2020, 12, 13982.
- [17] A. D. Jodlowski et al., *Nat. Energy*, 2017, 2, 972.
- [18] F. B. Minussi et al., *Chem. Commun.*, 2022, 58, 2212